Diffraction by Photomasks

Dr. Apo Sezginer
Weitao Chen, Jens Christian Jorgensen, Dennis Moore
Anton Sakovich, Shirin Sardar, Hsiao-Chieh Tseng

August 12, 2011

1 Introduction

Integrated circuits are produced at smaller and smaller scales to make more powerful electronic devices. According to Moore's law, the number of components in an integrated circuit will double every two years. Currently, the level of detail is at the nanometer scale, which presents many challenges.

At present, integrated circuits are produced by optical lithography. Specifically, light is passed through a photomask and an image of the mask is projected onto a photoresist to etch the desired patterns. Designing and inspecting a photomask for defects require accurately calculating the change in the electric field caused by the photomask. To be practical, this computation must be very quick.

The current lithography process uses deep ultraviolet light, but new technology is needed to increase the resolution. One likely alternative is to switch to extreme ultraviolet light, which has a shorter wavelength; however, at this wavelength materials are not very reflective or transparent. To get around this, two materials are alternately layered to produce a Bragg reflector. The photomask consists of an patterned absorber on top of a Bragg reflector.

Our goal is to find an efficient way to calculate the electromagnetic field after light has been reflected by the photomask.

In the first section, we determine the reflected and transmitted field for the multilayered reflector, using matrices to model the field in each layer of the reflector. Next, we compute the transmitted field at the bottom of a cross section of a thick absorptive material in terms of the incident field using an adaptation of the Born approximation. We have implemented the computations in Matlab to determine the accuracy. We conclude with a comparison of our results to a solution obtained using the finite element method (FEM). We also include an appendix covering Green's functions for the Helmholtz equation.

2 Multilayer Reflector

We start by modeling the transmission and reflection of extreme ultraviolet light by the multi-layered Bragg reflector. We first consider a more general problem: electromagnetic plane waves incident to N layers of arbitrary materials with specified thicknesses, d_1, d_2, …, d_N, and indices of refraction n_1, n_2, …, n_N. We assume that the materials only vary in one direction (say downward) and are homogeneous in perpendicular cross-sections. To further simplify the problem, we decompose the incident field into two orthogonal components, S-polarization and P-polarization, and treat these cases separately.

Let $\boldsymbol{E}_\mathrm{a}$, $\boldsymbol{E}_\mathrm{b}$, $\boldsymbol{E}_\mathrm{c}$, and $\boldsymbol{E}_\mathrm{d}$ be the total transmitted and reflected waves in the j-th and $j+1$-st layers, as illustrated in the following figure. We also establish a coordinate system in $\widehat{\boldsymbol{x}}$, $\widehat{\boldsymbol{y}}$, and $\widehat{\boldsymbol{z}}$, where $\widehat{\boldsymbol{x}}$ is to the right, $\widehat{\boldsymbol{y}}$ is pointing into the page, and $\widehat{\boldsymbol{z}}$ is up.

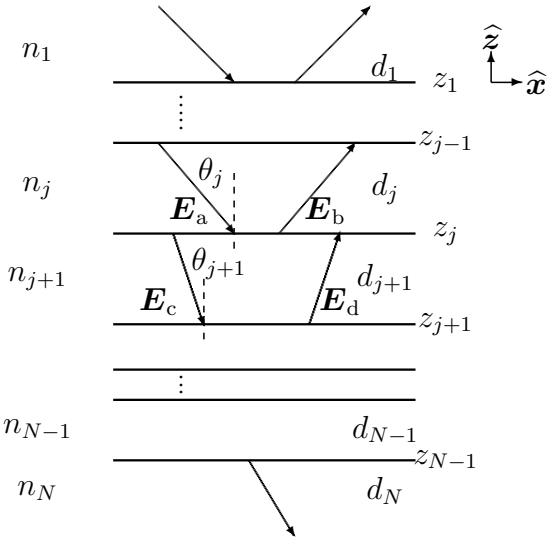

Figure 1: multilayer structure

Assume the plane of incidence is spanned by $\widehat{\boldsymbol{x}}$ and $\widehat{\boldsymbol{z}}$, and that t_j, r_j are, respectively, the down-going and up-going wave coefficients at the j-th boundary between media. For the S-polarization plane electromagnetic wave, set

$$\boldsymbol{E}_\mathrm{a} = t_j \widehat{\boldsymbol{y}} \mathrm{e}^{\mathrm{i}\boldsymbol{k}_\mathrm{a}\cdot\boldsymbol{x}} \qquad \boldsymbol{E}_\mathrm{b} = r_j \widehat{\boldsymbol{y}} \mathrm{e}^{\mathrm{i}\boldsymbol{k}_\mathrm{b}\cdot\boldsymbol{x}} \qquad \boldsymbol{E}_\mathrm{c} = t_{j+1} \widehat{\boldsymbol{y}} \mathrm{e}^{\mathrm{i}\boldsymbol{k}_\mathrm{c}\cdot\boldsymbol{x}} \qquad \boldsymbol{E}_\mathrm{d} = r_{j+1} \widehat{\boldsymbol{y}} \mathrm{e}^{\mathrm{i}\boldsymbol{k}_\mathrm{d}\cdot\boldsymbol{x}}$$

$$\boldsymbol{k}_\mathrm{a} = \begin{bmatrix} k_{x,j} \\ 0 \\ -k_{z,j} \end{bmatrix} \qquad \boldsymbol{k}_\mathrm{b} = \begin{bmatrix} k_{x,j} \\ 0 \\ +k_{z,j} \end{bmatrix} \qquad \boldsymbol{k}_\mathrm{c} = \begin{bmatrix} k_{x,j+1} \\ 0 \\ -k_{z,j+1} \end{bmatrix} \qquad \boldsymbol{k}_\mathrm{d} = \begin{bmatrix} k_{x,j+1} \\ 0 \\ +k_{z,j+1} \end{bmatrix}$$

where $k_j^2 = \omega^2 \mu_0 \epsilon_j = k_{x,j}^2 + k_{z,j}^2$ and

$$k_{x,j} = k_j \sin\theta_j \in \mathbb{R}$$

$$k_{z,j} = k_j \cos\theta_j = \sqrt{k_j^2 - k_x^2} = \sqrt{n_j^2 \left(\frac{2\pi}{\lambda}\right)^2 - k_x^2}$$

for $j = 1, \ldots, N$ with the branch of the square root being chosen such that the imaginary part is nonnegative. Since $\widehat{\boldsymbol{n}} \times \boldsymbol{E}$ is continuous at each interface $z = z_j$, the total fields immediately above and below the boundary must be equal, so we have

$$t_j \mathrm{e}^{\mathrm{i}k_{x,j}x - \mathrm{i}k_{z,j}z_j} + r_j \mathrm{e}^{\mathrm{i}k_{x,j}x + \mathrm{i}k_{z,j}z_j} = t_{j+1}\mathrm{e}^{\mathrm{i}k_{x,j+1}x - \mathrm{i}k_{z,j+1}z_j} + r_{j+1}\mathrm{e}^{\mathrm{i}k_{x,j+1}x + \mathrm{i}k_{z,j+1}z_j} \tag{1}$$

for the x-components, whereas the y and z-components are zero. Note that the above equation holds for all $x \in \mathbb{R}$, so $k_{x,j} = k_{x,j+1} = k_x$ for all j. In case ϵ_j is positive and $|k_{x,j}| < k_j$, then $k_{x,j} = k_j \sin\theta_j$ and $k_{z,j} = k_j \cos\theta_j$. Then, $k_{x,j} = k_{x,j+1}$ gives *Snell's law*:

$$k_j \sin\theta_j = k_{j+1}\sin\theta_{j+1}$$

for all j.

This branch corresponds to waves that decay in the direction of propagation. Using these constants, we can rewrite (1) as

$$t_j \mathrm{e}^{-\mathrm{i}k_{z,j}z_j} + r_j \mathrm{e}^{\mathrm{i}k_{z,j}z_j} = t_{j+1}\mathrm{e}^{-\mathrm{i}k_{z,j+1}z_j} + r_{j+1}\mathrm{e}^{\mathrm{i}k_{z,j+1}z_j} \tag{2}$$

Once the time-harmonic electric fields $\boldsymbol{E}_\mathrm{a}$, $\boldsymbol{E}_\mathrm{b}$, $\boldsymbol{E}_\mathrm{c}$, and $\boldsymbol{E}_\mathrm{d}$ are known, the corresponding magnetic fields $\boldsymbol{H}_\mathrm{a}$, $\boldsymbol{H}_\mathrm{b}$, $\boldsymbol{H}_\mathrm{c}$, and $\boldsymbol{H}_\mathrm{d}$ can be determined by one of Maxwell's equations

$$\nabla \times \boldsymbol{E} = \mathrm{i}\omega\mu_0 \boldsymbol{H}$$

This gives the following equations

$$\boldsymbol{H}_\mathrm{a} = \frac{t_j}{\omega\mu_0}\begin{bmatrix} k_{z,j} \\ 0 \\ k_x \end{bmatrix} \mathrm{e}^{\mathrm{i}\boldsymbol{k}_a\cdot\boldsymbol{x}} \qquad \boldsymbol{H}_\mathrm{b} = \frac{r_j}{\omega\mu_0}\begin{bmatrix} -k_{z,j} \\ 0 \\ k_x \end{bmatrix} \mathrm{e}^{\mathrm{i}\boldsymbol{k}_b\cdot\boldsymbol{x}}$$

$$\boldsymbol{H}_\mathrm{c} = \frac{t_{j+1}}{\omega\mu_0}\begin{bmatrix} k_{z,j+1} \\ 0 \\ k_x \end{bmatrix} \mathrm{e}^{\mathrm{i}\boldsymbol{k}_c\cdot\boldsymbol{x}} \qquad \boldsymbol{H}_\mathrm{d} = \frac{r_{j+1}}{\omega\mu_0}\begin{bmatrix} -k_{z,j+1} \\ 0 \\ k_x \end{bmatrix} \mathrm{e}^{\mathrm{i}\boldsymbol{k}_d\cdot\boldsymbol{x}}$$

We may now apply continuity of $\widehat{\boldsymbol{n}} \times \boldsymbol{H}$ on each interface, to get

$$t_j k_{z,j}\mathrm{e}^{-\mathrm{i}k_{z,j}z_j} - r_j k_{z_j}\mathrm{e}^{\mathrm{i}k_{z,j}z_j} = t_{j+1}k_{z,j+1}\mathrm{e}^{-\mathrm{i}k_{z,j+1}z_j} - r_{j+1}k_{z,j+1}\mathrm{e}^{\mathrm{i}k_{z,j+1}z_j} \tag{3}$$

We can rewrite (2) and (3) as a linear system:

$$\begin{bmatrix} 1 & 1 \\ k_{z,j} & -k_{z,j} \end{bmatrix}\begin{bmatrix} \mathrm{e}^{-\mathrm{i}k_{z,j}z_j} & 0 \\ 0 & \mathrm{e}^{\mathrm{i}k_{z,j}z_j} \end{bmatrix}\begin{bmatrix} t_j \\ r_j \end{bmatrix} = \begin{bmatrix} 1 & 1 \\ k_{z,j+1} & -k_{z,j+1} \end{bmatrix}\begin{bmatrix} \mathrm{e}^{-\mathrm{i}k_{z,j+1}z_j} & 0 \\ 0 & \mathrm{e}^{\mathrm{i}k_{z,j+1}z_j} \end{bmatrix}\begin{bmatrix} t_{j+1} \\ r_{j+1} \end{bmatrix}$$

This can now be simplified by letting

$$\boldsymbol{u}_j = \begin{bmatrix} \mathrm{e}^{-\mathrm{i}k_{z,j}z_j} & 0 \\ 0 & \mathrm{e}^{\mathrm{i}k_{z,j}z_j} \end{bmatrix}\begin{bmatrix} t_j \\ r_j \end{bmatrix} \qquad M_j = \begin{bmatrix} 1 & 1 \\ k_{z,j} & -k_{z,j} \end{bmatrix} \qquad D_j = \begin{bmatrix} \mathrm{e}^{-\mathrm{i}k_{z,j}d_j} & 0 \\ 0 & \mathrm{e}^{\mathrm{i}k_{z,j}d_j} \end{bmatrix}$$

where $d_j = z_j - z_{j+1}$ is the thickness of the j-th layer, which gives the recursive relation

$$\boldsymbol{u}_j = M_j^{-1} M_{j+1} D_{j+1} \boldsymbol{u}_{j+1} \qquad j = 1, 2, \ldots, N-1 \tag{4}$$

We now can obtain the electric field on one side of an interface in terms of the electric field on the other side, and we can determine the electric field across any number of layers by multiplying the appropriate matrices, called transfer matrices.

To determine the electric field in an arbitrary layer, we observe that there is no up-going wave field in the last layer, or, equivalently, setting $r_N = 0$ and $\boldsymbol{u}_N = (1, 0)^\intercal$ for the last layer, and work up to the desired layer.

In the simplest case, we have only two layers. Suppose $z_1 = 0$ is the interface between two media with refractive indices n_1 and n_2. Again, we set $\boldsymbol{u}_2 = (t_2, r_2)^\intercal = (1, 0)^\intercal$, in (4) to obtain t_1 and r_1. If we normalize t_1 to unity, this yields the Fresnel equations

$$t_2 = \frac{2k_{z,1}}{k_{z,1} + k_{z,2}} \qquad r_1 = \frac{k_{z,1} - k_{z,2}}{k_{z,1} + k_{z,2}}.$$

The total field actually consists of multiple scattering waves inside each layer. We can demonstrate this by taking just one layer and considering the reflected and transmitted field as figure 2 shows.

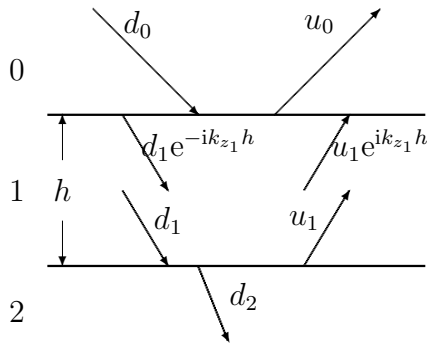

Figure 2: wave from medium 0 going through medium 1 to medium 2

Total fields above the layer, inside the layer and below the layer should satisfy the following equations.

$$u_0 = r_{01} d_0 + t_{10} u_1 e^{ik_{z_1}h} \tag{5}$$

$$d_1 e^{-ik_{z_1}h} = t_{01} d_0 + r_{10} u_1 e^{ik_{z_1}h} \tag{6}$$

$$u_1 = r_{12} d_1 \tag{7}$$

$$d_2 = t_{12} d_1 \tag{8}$$

where r_{ij}, t_{ij} denotes the reflection and transmission coefficients through the interface from medium i to j respectively, k_{z1} is the z component of the wave vector in medium 1.

Solving (5)-(8) for u_0/d_0, we find

$$\begin{aligned}\frac{u_0}{d_0} &= r_{01} + t_{10}e^{ik_{z1}h}\frac{t_{01}r_{12}\mathrm{e}^{\mathrm{i}k_{z1}h}}{1 - r_{12}r_{10}\mathrm{e}^{2\mathrm{i}k_{z1}h}} \\ &= r_{01} + t_{10}t_{01}r_{12}\mathrm{e}^{2\mathrm{i}k_{z1}h}\sum_{j=0}^{\infty}(r_{12}r_{10}\mathrm{e}^{2\mathrm{i}k_{z1}h})^j\end{aligned}$$

Consider the general term in the geometric series, $t_{10}t_{01}r_{12}\mathrm{e}^{2\mathrm{i}k_{z1}h}(r_{12}r_{10}\mathrm{e}^{2\mathrm{i}k_{z1}h})^j$. It actually describes the wave which is reflected $2j+1$ times inside the layer and then transmitted through the top.

Similarly, we can calculate the total transmission below the layer compared with the incident wave.

$$\begin{aligned}\frac{d_2}{d_0} &= \frac{t_{12}u_1}{r_{12}d_0} \\ &= \frac{t_{01}t_{12}\mathrm{e}^{\mathrm{i}k_{z1}h}}{1 - r_{12}r_{10}\mathrm{e}^{2\mathrm{i}k_{z1}h}} \\ &= t_{01}t_{12}\mathrm{e}^{\mathrm{i}k_{z1}h}\sum_{j=0}^{\infty}(r_{12}r_{10}\mathrm{e}^{2\mathrm{i}k_{z1}h})^j\end{aligned}$$

Consider the general term in the geometric series, $t_{01}t_{12}\mathrm{e}^{\mathrm{i}k_{z,1}h}(r_{12}r_{10}\mathrm{e}^{2\mathrm{i}k_{z,1}h})^j$, it is just the wave reflected $2j$ times inside the layer and then transmitted through the bottom.

Thus by the transfer-matrix method, we solve the total field containing multiple scattering waves.

Now that we have solved the general problem of reflection and transmission through many layers, we can return to the specific case we are interested in. For the Bragg reflector, the layers alternate between two materials–molybdenum and silicon– (plus a capping layer of ruthenium at the top), and the layers of the respective materials all have the same thickness, so there are only three different 2×2 matrices involved in the computation. Thus, this step of the process can be calculated very quickly.

3 Transmission Matrix for the Absorber

In this section, we describe difraction of S-polarized plane waves by an absorbing body. Let us consider an absorber that stretches infinitely along the y-axis and has a rectangular cross-section in the xz-plane. Let us also assume that the incident plane wave hits the absorber at a small angle. The geometry for the S-polarized waves and an infinitely long absorber is simple; however, the ideas we describe here form a building block for simulating diffraction in more complicated settings.

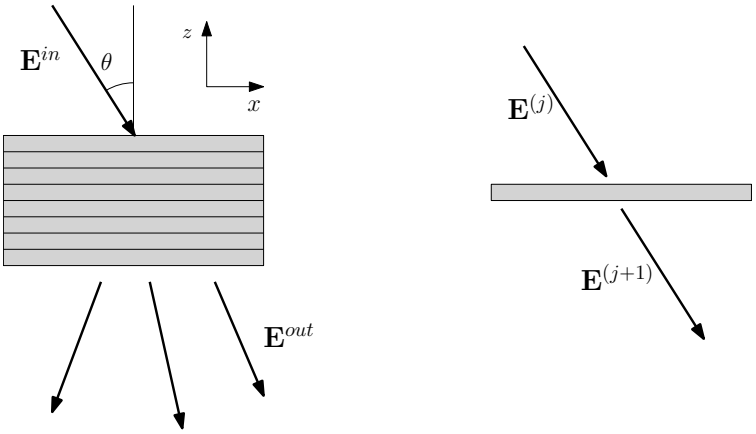

Figure 3: Sliced absorber with incident and transmitted waves (left). Incomming and outgoing waves on $(j+1)$st slice.

We use a perturbation approach to solving for the electromagnetic field known as the Born approximation. Let us note, however, that we adapt the method for our needs. To make sure the Born approximation is accurate, we need to take care of two things. First, we assume that permittivity of the absorber is nearly the same as that of the vacuum. This allows us to use the solutions of Maxwell's equations as a leading order contribution to the solution. Next, to make sure the variation of the field is small in our solution scheme, we successively find the solution on boundaries of thin rectangular slices of the absorber moving down along the z-axis (see Figure 3).

3.1 Perturbation Approach

As an electromagnetic wave propagates along the absorber, it experiences only small variation in each of the slices shown on Figure 3. Using the perturbation techniques we derive a method for computing the field inside each slice given the field at its top surface.

Let us assume that the permittivity of the absorber, ϵ, is varying only in the $\hat{x}$ and $\hat{z}$ directions. The electromagnetic field is governed by the time-harmonic Maxwell's equations

$$\nabla \times \boldsymbol{E} = \mathrm{i}\omega\mu_0 \boldsymbol{H} \tag{9}$$
$$\nabla \times \boldsymbol{H} = -\mathrm{i}\omega\epsilon \boldsymbol{E} \tag{10}$$

where permittivity is $\epsilon = \epsilon_0 + \delta\epsilon$, and ϵ_0 and μ_0 are constant permittivity and permeability of vacuum. Assuming that $|\delta\epsilon| \ll \epsilon_0$, let us look for $\mathbf{E}$ and $\mathbf{H}$ in a small neighborhood of the incident field $\mathbf{E}_0$**,** $\mathbf{H}_0$. Let us write the solution in the form $\boldsymbol{E} = \boldsymbol{E}_0 + \delta\boldsymbol{E}$, $\boldsymbol{H} = \boldsymbol{H}_0 + \delta\boldsymbol{H}$, where $\boldsymbol{E}_0$, $\boldsymbol{H}_0$ are the electromagnetic waves in vacuum satisfying

$$\nabla \times \boldsymbol{E}_0 = \mathrm{i}\omega\mu_0 \boldsymbol{H}_0 \tag{11}$$
$$\nabla \times \boldsymbol{H}_0 = -\mathrm{i}\omega\epsilon_0 \boldsymbol{E}_0 \tag{12}$$

Taking the curl of (12) we find that $\mathbf{E}_0$ is divergence-free. Now, using equations (9) and (10) for the free field, we rewrite (9) and (10) in the following form:

$$\nabla \times \delta\boldsymbol{E} = \mathrm{i}\omega\mu_0 \delta\boldsymbol{H} \tag{13}$$
$$\nabla \times \delta\boldsymbol{H} = -\mathrm{i}\omega \left(\epsilon_0 \delta\boldsymbol{E} + \boldsymbol{E}_0 \delta\epsilon + \delta\epsilon \cdot \delta\boldsymbol{E}\right) \tag{14}$$

For a thin slice, $\delta\mathbf{E}$ is small, so we can drop the second-order term $\delta\epsilon \cdot \delta\boldsymbol{E}$. By taking the curl of (13), we eliminate the magnetic field and find the equation for the first order correction to the $\mathbf{E}$-field:

$$\nabla \times \nabla \times \delta\boldsymbol{E} = \omega^2 \mu_0 \epsilon_0 \delta\boldsymbol{E} + \omega^2 \mu_0 \boldsymbol{E}_0 \delta\epsilon \tag{15}$$

Taking the divergence of (14) we find that

$$\nabla \cdot \delta\boldsymbol{E} = -\frac{1}{\epsilon_0} \boldsymbol{E}_0 \cdot \nabla\delta\epsilon$$

Since the incident field $\boldsymbol{E}_0$ is S-polarized and $\nabla\delta\epsilon$ lies in xz-plane, we have $\boldsymbol{E}_0 \cdot \nabla\delta\epsilon = 0$. Finally, using the identity $\nabla \times \nabla \times \delta\boldsymbol{E} = -\Delta\delta\boldsymbol{E} + \nabla(\nabla \cdot \delta\boldsymbol{E})$, we reduce equation (15) to the Helmholtz equation

$$\left(\Delta + k_0^2\right) \delta\boldsymbol{E} = -k_0^2 \frac{\delta\epsilon}{\epsilon_0} \boldsymbol{E}_0 \tag{16}$$

where $k_0 = 2\pi/\lambda$ is the wave number of the incident wave. Clearly, this equation can be solved using the Green's function for the operator $\Delta + k_0^2$, thus providing the solution $\mathbf{E} = \mathbf{E}_0 + \delta\mathbf{E}$ in the first slice.

It is important to point out that equation (16) can be used to solve for the field in a slab of absorber. Let z_j denote the height of the jth slice top surface, with j increasing as we go down along z-axis. Let us also decompose the electromagnetic field and permittivity in

$(j+1)$st slice as $\mathbf{E}^{[j+1]} = \mathbf{E}^{[j]} + \delta\mathbf{E}^{[j+1]}$. Then, the iterative scheme for finding the solution for the sliced Born approximation can be written as

$$\left(\Delta + k_0^2\right)\delta\boldsymbol{E}^{[j+1]} = -k_0^2\frac{\delta\epsilon}{\epsilon_0}\boldsymbol{E}^{[j]} \qquad \mathbf{E}^{[j+1]} = \mathbf{E}^{[j]} + \delta\mathbf{E}^{[j+1]} \tag{17}$$

This approximation ignores the reflection off of other slabs (multiple scattering), in addition to the second order term in equation (14).

3.2 Updating the Field between Slices

In this section, we prepare for the numerical computation of the electromagnetic field in the presence of absorber. We derive the explicit expression for the field perturbations $\{\delta\mathbf{E}^{[j]}\}$ in equation (17) and discuss the cost of its numerical computation.

Suppose we have an S-polarized wave with electromagnetic field $\mathbf{E}$ hitting a thin absorber of thickness d. We find the electromagnetic field inside the slice in Born approximation by adding $\delta\mathbf{E}$, found from (17), to the incoming field. Solving the inhomogeneous equation (17) we get

$$\delta\mathbf{E}(\boldsymbol{x}) = \frac{k_0^2}{\epsilon_0}\int_\Omega g_0(\boldsymbol{x},\boldsymbol{x}')\delta\epsilon(x')\mathbf{E}(\boldsymbol{x}')\,\mathrm{d}\boldsymbol{x}' \tag{18}$$

where $\Omega = \mathbb{R}^2 \times [0,d]$ and g_0 is the free-space Green's function satisfying the Helmholtz equation $\Delta g_0 + k_0^2 g_0 = -\delta(\boldsymbol{x},\boldsymbol{x}')$ in 3-D:

$$g_0(\boldsymbol{x},\boldsymbol{x}') = \frac{\mathrm{e}^{\mathrm{i}k_0|\boldsymbol{x}-\boldsymbol{x}'|}}{4\pi\,|\boldsymbol{x}-\boldsymbol{x}'|} = -\int_{\mathbb{R}^2}\frac{\mathrm{e}^{\mathrm{i}k_x'(x-x')+\mathrm{i}k_y'(y-y')+\mathrm{i}k_z'|z-z'|}}{8\pi^2\mathrm{i}k_z'}\,\mathrm{d}k_x'\,\mathrm{d}k_y'$$

with $k_z' = \sqrt{k_0^2-(k_x')^2-(k_y')^2}$. To proceed with numerical computations, we assume that the absorber is periodic in the x direction with period p, where p is large. (This gives reasonable boundary conditions.) We can then write

$$\delta\epsilon(\mathbf{x}) = \epsilon_0(n_A^2-1)q(\mathbf{x})$$

where n_A is the index of refraction of the absorber, and $q(\mathbf{x}+\hat{x}p) = q(\mathbf{x})$. Note, however, that the geometry of the absorber does not have to be restricted to that shown in Figure 3.

We expand the structure function q in Fourier modes, $q(x) = \sum_{n=-\infty}^{\infty} c_n \mathrm{e}^{\mathrm{i}\frac{2\pi n}{p}x}$, and use the Bloch-periodic ansatz for the electromagnetic field:

$$E(\boldsymbol{x}) = E(x,z) = \sum_{n=-\infty}^{\infty} E_n \mathrm{e}^{\mathrm{i}k_{x,n}x - \mathrm{i}k_{z,n}z} \qquad \delta E(\boldsymbol{x}) = \delta E(x,z) = \sum_{n=-\infty}^{\infty}\delta E_n \mathrm{e}^{\mathrm{i}k_{x,n}x-\mathrm{i}k_{z,n}z}$$

where $k_{x,n} = k_0\sin\theta + \frac{2\pi n}{p}$, $k_{z,n} = \sqrt{k_0^2-k_{x,n}^2}$, and E stands for the y-component of the field. With the above expansions for the incident field, permittivity and Green's function, formula (18) yields the following value of the field at the bottom of the slice

$$\begin{aligned}
\delta E(x,z) &= -k_0^2(n_A^2-1)\int_\Omega\int_{\mathbb{R}^2} \frac{\mathrm{e}^{\mathrm{i}k_x'(x-x')+\mathrm{i}k_y'(y-y')+\mathrm{i}k_z'|z-z'|}}{8\pi^2\mathrm{i}k_z'} \sum_{m,n=-\infty}^{\infty} c_m E_n \mathrm{e}^{\mathrm{i}k_{x,n+m}x'-\mathrm{i}k_{z,n}z'}\,\mathrm{d}k_x'\,\mathrm{d}k_y'\;\mathrm{d}\boldsymbol{x}' \\
&= -\frac{k_0^2(n_A^2-1)}{8\pi^2\mathrm{i}} \sum_{m,n=-\infty}^{\infty} \int_0^d\int_{\mathbb{R}^2} \mathrm{e}^{\mathrm{i}(k_x'x+k_y'y+k_z'|z-z'|-k_{z,n}z')} c_{m-n}E_n(2\pi)^2\delta(k_{x,m}-k_x')\delta(-k_y')\frac{\mathrm{d}k_x'\,\mathrm{d}k_y'}{k_z'}\,\mathrm{d}z' \\
&= -\frac{k_0^2(n_A^2-1)}{2\mathrm{i}} \sum_{m,n=-\infty}^{\infty} c_{m-n}E_n \frac{\mathrm{e}^{\mathrm{i}k_{x,m}x-\mathrm{i}k_{z,m}z}}{k_{z,m}} \int_0^d \mathrm{e}^{\mathrm{i}(k_{z,m}-k_{z,n})z'}\,\mathrm{d}z' \qquad (\ z'>z\ )
\end{aligned}$$

The integration in z' can be explicitly calculated via a sinc function. By comparing the series coefficients, we find a correction for mth Bloch mode:

$$\delta E_m = -\frac{k_0^2(n_A^2-1)d}{2\mathrm{i}} \sum_{n=-\infty}^{\infty} c_{m-n}\frac{\mathrm{e}^{\mathrm{i}(k_{z,m}-k_{z,n})d/2}}{k_{z,m}}\operatorname{sinc}((k_{z,m}-k_{z,n})d/2)E_n \tag{19}$$

At the bottom of the slice, the resulting electric field is computed by the following formula

$$E^{[j+1]}(x,z) = E^{[j]}(x,z) + \delta E[j+1](x,z)$$

and advancing each mode of $E^{[j+1]}(x,z)$ by a factor of $e^{ik_{z,m}d}$.

This can also be written as an iterative formula in the frequency domain:

$$E_m^{[j+1]} = \sum_{n=-\infty}^{\infty} \mathrm{e}^{\mathrm{i}k_{z,m}d}[I+M(d)]_{m,n}E_n^{[j]} \tag{20}$$

where I is the identity matrix, and the coefficients of matrix M are given by

$$[M(d)]_{m,n} = -\frac{k_0^2(n_A^2-1)d}{2\mathrm{i}}c_{m-n}\frac{\mathrm{e}^{\mathrm{i}(k_{z,m}-k_{z,n})d/2}}{k_{z,m}}\operatorname{sinc}((k_{z,m}-k_{z,n})d/2) \tag{21}$$

The operation of updating the field is not a convolution because the matrix M depends on $k_{z,m}-k_{z,n}$. Hence, to compute the field using (20), we need to work out $\mathcal{O}(N^2)$ operation, with N being the size of the matrix, or the number of truncated Fourier modes $m,n\in[-N/2,\ldots,N/2]$. To imrove the speed of computations, we expand the elements of matrix M in the small parameter d in a Taylor series. We observe that $\mathrm{e}^{\mathrm{i}(k_{z,m}-k_{z,n})d}\approx 1+\mathrm{i}(k_{z,m}-k_{z,n})d$ by the first order Taylor approximation and

$$\mathrm{e}^{\mathrm{i}(k_{z,m}-k_{z,n})d/2}\operatorname{sinc}((k_{z,m}-k_{z,n})d/2) = d^{-1}\frac{\mathrm{e}^{\mathrm{i}(k_{z,m}-k_{z,n})d}-1}{\mathrm{i}(k_{z,m}-k_{z,n})} \approx 1$$

provided $|k_{z,m}-k_{z,n}|\,|d|\ll 1$. Since $|k_{z,n}|^2 = \left|k_0^2-(k_0+\frac{2\pi n}{p})^2\right| \le C\cdot\pi\frac{N}{p}$, the approximations give a good result, provided $d\ll\frac{p}{2\pi N}$. The matrix M can be replaced, using these approximations, by

$$[\tilde{M}(d)]_{m,n} = -\frac{k_0^2(n_A^2-1)d}{2\mathrm{i}}\frac{c_{m-n}}{k_{z,m}} \tag{22}$$

The computation of the field with this matrix involves $\mathcal{O}(N \log_2 N)$ operations.

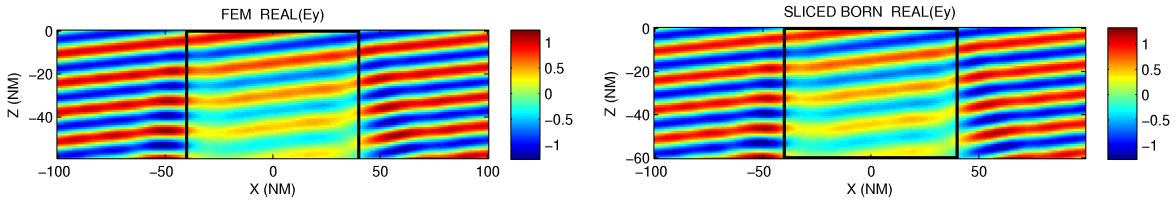

Figure 4: The simulation of real parts of the total field obtained by sliced Born and FEM with incident wavelength 13.5 nm only containing a single mode 0 in Fourier space. The scatterer is a periodic array of 60 nm thick, 80 nm wide, infinitely long strips of TaBN ($n_A = 0.91654 + 0.04375\mathrm{i}$), with period 200 nm, the angle of incidence being 6 deg. No Bragg reflector is present.

Comparing the result of the sliced Born approximation with FEM, the profiles are quite similar; we show the error between them in figure 5. The first two figures are generated by the Born approximation with the exact matrix (21). The solution of the sliced Born approximation converges as the number of slices is increased and the absolute error of these two methods decreases. However, the error stagnates at 5% of the incident field amplitude when there are more than 50 slices. This illustrates that the sliced Born approximation gives us a convergent solution with some small error ($< 10^{-1}$). Running time increases a little bit, but not significantly, for more slices. The last two figures in figure 5 are generated by the sliced Born approximation with the approximate matrix (22). Since we can write this operation as a convolution, the running time is decreased while the convergence rate and error remain almost the same.

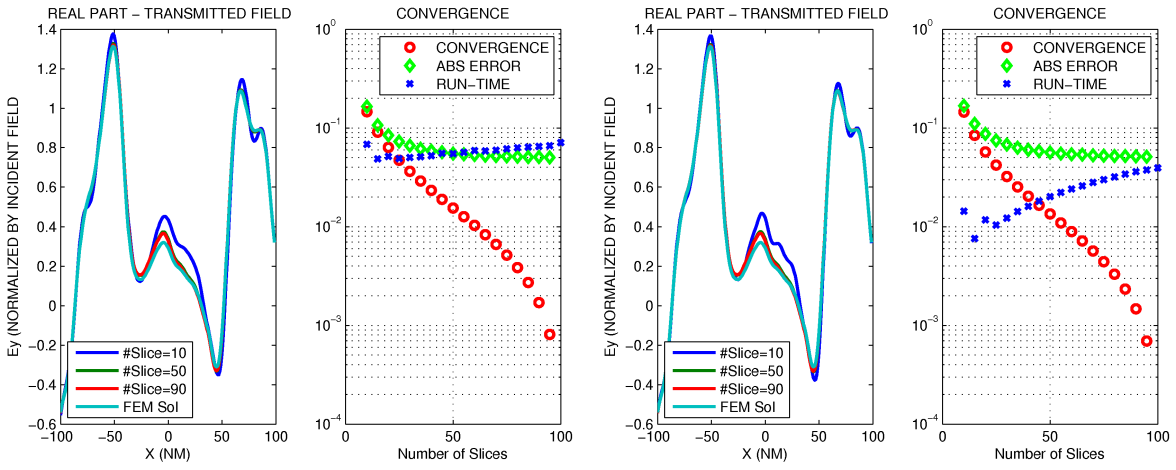

Figure 5: The comparison of the sliced Born and FEM simulations of transmitted fields passing through the absorber (with no Bragg reflector), and the convergent tests for the sliced Born with fixed number of Fourier modes. The sliced Born iteration is applied by the matrix (21) (left) and (22) (right).

4 Simulation Procedure for the Photomask Diffraction

The whole diffraction process is as follows: An EUV wave, say S-polarized, passes through the absorber, is reflected by the Bragg reflector under the absorber, and passes through the absorber again.

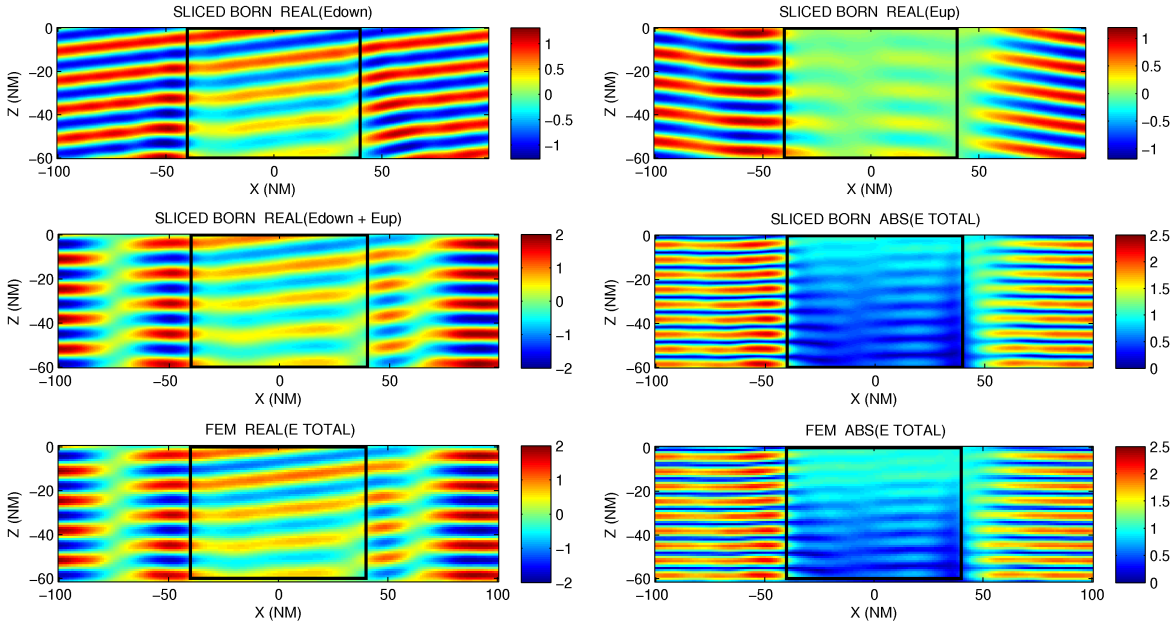

Figure 6: The plots of S-polarized wave fields using sliced Born approximation (first two rows) and FEM (the last row).

Figure 6 shows the profiles in one period of the absorber when the wave completes the entire process. The last two rows show that the sliced Born approximation and FEM give very similar total fields.

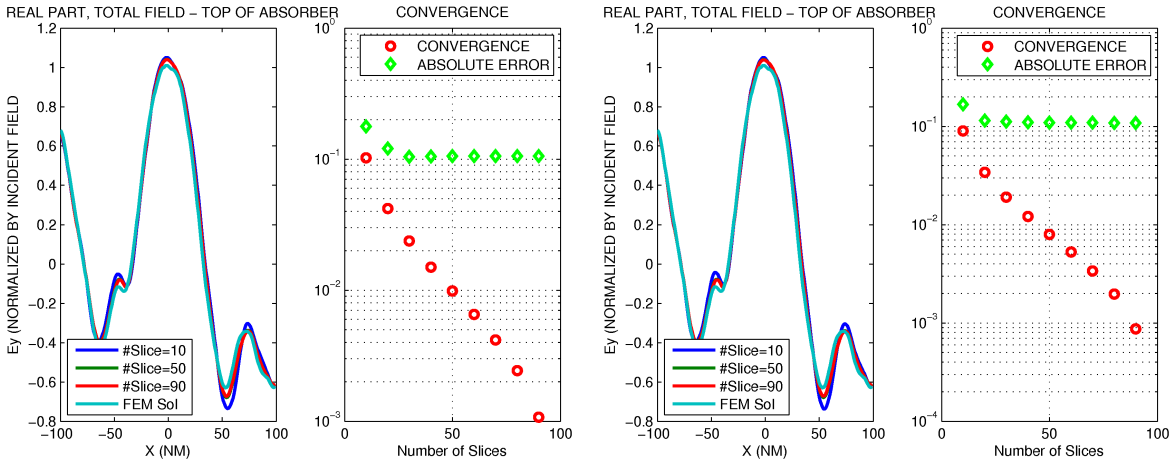

Figure 7: Comparison of the transmitted field on the top of the absorber after the absortion, transmition, and reflection process. The sliced Born iteration is applied by the exact matrix (21) (left) and the approximate matrix (22) (right).

We show the error and convergence of the Born approximation for the whole process in figure 7. We can see that the method is convergent and the limit solution is within 10% of the FEM solution for the incident field amplitude.

5 P-polarization

With the same assumptions on the absorber (say, it is inhomogeneous and p-periodic in the x direction), the above methods can be applied to a P-polarized plane wave; however, the gradient of $\delta\epsilon = \delta\epsilon(x)$ is no longer perpendicular to $\boldsymbol{E}$. More explicitly, the P-polarized incident field is of the following form

$$\boldsymbol{E}^{[0]}(x,z) = \begin{bmatrix} \cos\theta \\ 0 \\ \sin\theta \end{bmatrix} \mathrm{e}^{\mathrm{i}k_{x,0}x - \mathrm{i}k_{z,0}z},$$

and the electric field interacting with the absorber is then Bloch periodic:

$$\boldsymbol{E}(x,z) = \sum_{n=-\infty}^{\infty} \boldsymbol{v}_n \mathrm{e}^{\mathrm{i}k_{x,n}x - \mathrm{i}k_{z,n}z}$$

where $\boldsymbol{v}_n$ is a vector sequence whose second component is zero;

The resulting equation for the perturbation field $\delta\boldsymbol{E}$ is of the form

$$\nabla \times \nabla \times \delta\boldsymbol{E} - k_0^2 \delta\boldsymbol{E} = \omega^2 \mu_0 \, \delta\boldsymbol{E} \, \boldsymbol{E}$$

and the solution can be represented by the vector Green's function (as shown in the appendix).

The numerical simulation is shown in figure 8, 9 and 10. By the profiles of the total fields in the x and z directions compared with FEM, we know the sliced Born method gives quite accurate results. The error can be observed numerically in figure 10. The calculated fields E_x and E_z differ from the FEM solution by 10% and 3.5%, respectively, of the incident field amplitude. The greatest error occurs at the edges of the absorber.

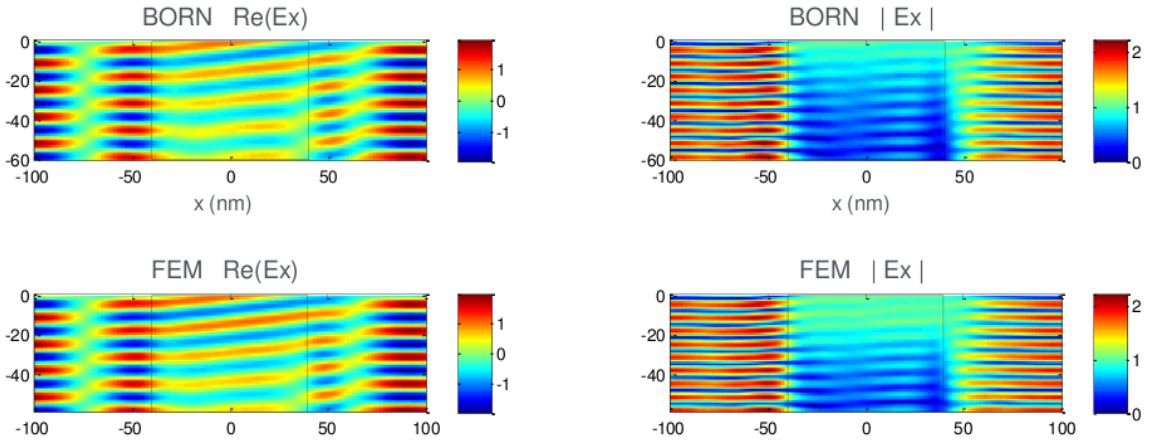

Figure 8: Agreement between FEM and sliced-Born with the reflector on E_x component.

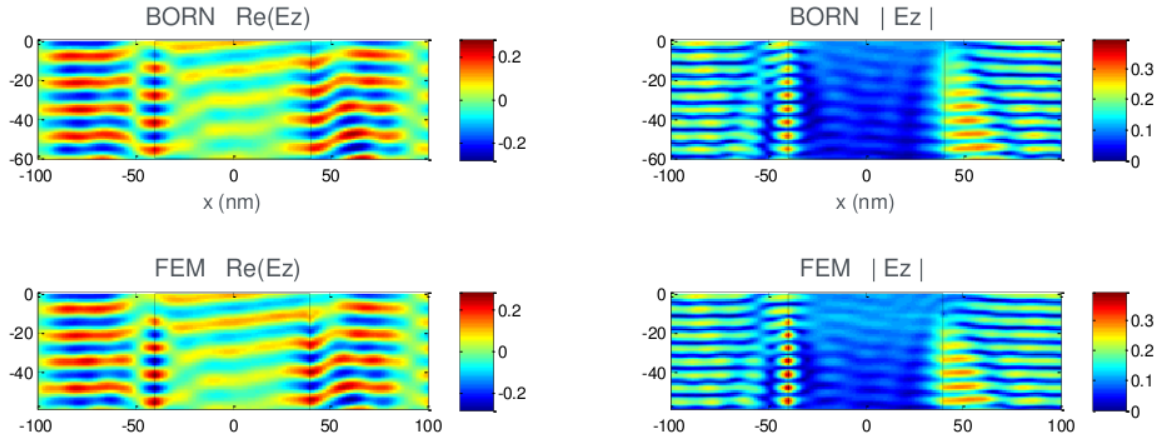

Figure 9: Agreement between FEM and sliced-Born with the reflector on E_z component.

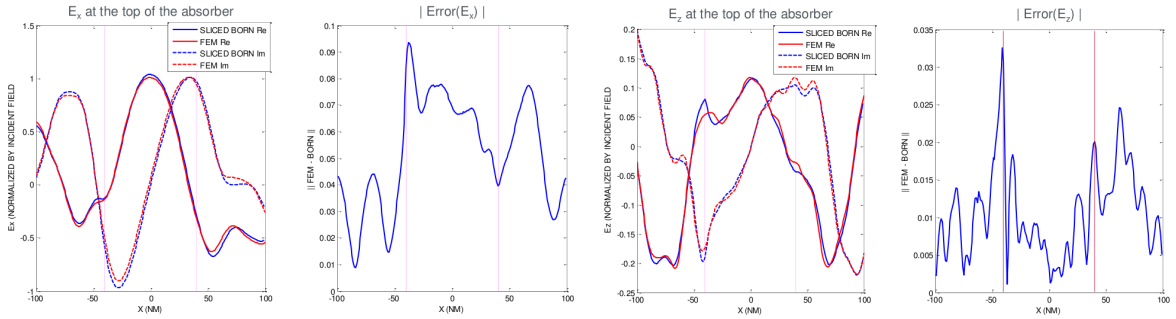

Figure 10: The comparison between FEM and sliced-Borm at the top of the absorber, for component E_x (left) and E_y (right) respectively. The largest relative error ($\approx 10\%$) occurs at the edge ($x = -40$nm) of the absorber.

6 Acknowledgements

Our team would like to thank the IMA and PIMS for their generous support for this experience. We would also like to thank our mentor, Dr. Apo Sezginer, for his expertise, patience, and encouragement.

A Appendix

A.1 Helmholtz Equations for Time Harmonic Maxwell Equations

Let's begin with the free space time-harmonic Maxwell equation with a current source $\boldsymbol{J}$:

$$\nabla \times \boldsymbol{E} = \mathrm{i}\omega\mu_0 \boldsymbol{H} \tag{23}$$
$$\nabla \times \boldsymbol{H} = -\mathrm{i}\omega\epsilon_0 \boldsymbol{E} + \boldsymbol{J} \tag{24}$$

where $\epsilon_0 = 8.85 \times 10^{-3}$[F/nm] and μ_0 are constant permittivity and permeability in vacuum. Taking divergence of (23) gives $\nabla \cdot \boldsymbol{H} = 0$, and thus

$$\boldsymbol{H} = \nabla \times \boldsymbol{A} \tag{25}$$

where $\boldsymbol{A}$ is a vector potential, and (23) yields $\nabla \times (\boldsymbol{E} - \mathrm{i}\omega\mu_0 \boldsymbol{A}) = 0$, or equivalently

$$\boldsymbol{E} - \mathrm{i}\omega\mu_0 \boldsymbol{A} = -\nabla\phi \tag{26}$$

for some scalar potential ϕ. Note that $(\boldsymbol{A}, \phi)$ determines $(\boldsymbol{E}, \boldsymbol{H})$.

Now take the curl of (24):

$$\begin{aligned} \nabla \times \boldsymbol{H} = \nabla \times \nabla \times \boldsymbol{A} \ &= \ \nabla(\nabla \cdot \boldsymbol{A}) - \Delta \boldsymbol{A} \\ &= -\mathrm{i}\omega\epsilon_0(\mathrm{i}\omega\mu_0 \boldsymbol{A} - \nabla\phi) + \boldsymbol{J}. \end{aligned}$$

By rearranging the terms and imposing the Gauge condition

$$\nabla \cdot \boldsymbol{A} - \mathrm{i}\omega\epsilon_0\phi = 0 \tag{27}$$

we have

$$(\Delta + k_0^2)\boldsymbol{A} = -\boldsymbol{J} \tag{28}$$

By taking divergence on (26), we see that

$$\nabla \cdot \boldsymbol{E} - \mathrm{i}\omega\mu_0 \nabla \cdot \boldsymbol{A} = -\Delta\phi$$

By (27) and taking $\nabla\cdot$ on (24), it gives

$$(\Delta + k_0^2)\phi = -\nabla \cdot \boldsymbol{E} = -\frac{\nabla \cdot \boldsymbol{J}}{\mathrm{i}\omega\epsilon_0} \tag{29}$$

Equations (28) and (29) are Helmholtz equations, whose solution can be represented by the Green's function

$$\begin{aligned} \boldsymbol{A}(\boldsymbol{x}) &= \int g(\boldsymbol{x}, \boldsymbol{x}')\boldsymbol{J}(\boldsymbol{x}')\,\mathrm{d}\boldsymbol{x}' \\ \phi(\boldsymbol{x}) &= \frac{1}{\mathrm{i}\omega\epsilon_0} \int g(\boldsymbol{x}, \boldsymbol{x}')\nabla' \cdot \boldsymbol{J}(\boldsymbol{x}')\,\mathrm{d}\boldsymbol{x}' \end{aligned}$$

where $g(\boldsymbol{x}, \boldsymbol{x}') = g(\boldsymbol{x} - \boldsymbol{x}')$ is the Green's function for free space Helmholtz equation

$$(\Delta + k_0^2)g = -\delta$$

Once $\boldsymbol{A}$ and ϕ are solved, $\boldsymbol{E}$ and $\boldsymbol{H}$ are solved by their definition (26), (25). Note that, by the divergence theorem and the relation $\nabla' g(\boldsymbol{x}, \boldsymbol{x}') = -\nabla g(\boldsymbol{x}, \boldsymbol{x}')$, we have

$$\nabla \int g(\boldsymbol{x}, \boldsymbol{x}') \nabla' \cdot \boldsymbol{J}(\boldsymbol{x}') \, \mathrm{d}\boldsymbol{x}' = -\nabla \int (\nabla' g(\boldsymbol{x}, \boldsymbol{x}')) \cdot \boldsymbol{J}(\boldsymbol{x}') \, \mathrm{d}\boldsymbol{x}' = +\nabla \int \nabla g(\boldsymbol{x}, \boldsymbol{x}') \cdot \boldsymbol{J}(\boldsymbol{x}) \, \mathrm{d}\boldsymbol{x}'$$

So we have

$$\boldsymbol{E}(\boldsymbol{x}) = \mathrm{i}\omega\mu_0 \int \left[\left(I + \frac{\nabla\nabla}{k_0^2} \right) g(\boldsymbol{x}, \boldsymbol{x}') \right] \boldsymbol{J}(\boldsymbol{x}') \, \mathrm{d}\boldsymbol{x}' \tag{30}$$

$$\boldsymbol{H}(\boldsymbol{x}) = \int \left[\nabla g(\boldsymbol{x}, \boldsymbol{x}') \times \right] \boldsymbol{J}(\boldsymbol{x}') \, \mathrm{d}\boldsymbol{x}'. \tag{31}$$

A.2 Green's Function for 1D Helmholtz Equation

The 1D Helmholtz Equation is indeed an ODE, and the Green's function satisfies

$$\frac{\mathrm{d}^2}{\mathrm{d}z^2} g + k^2 g = -\delta(z)$$

The solution g is

$$g(z) = \frac{\mathrm{e}^{\mathrm{i}k|z|}}{-2\mathrm{i}k}$$

(One may check $\frac{\mathrm{d}}{\mathrm{d}z}|z| = \mathrm{sgn}(z)$, $\frac{\mathrm{d}}{\mathrm{d}z}\mathrm{sgn}(z) = 2\delta(z)$, and $\frac{\mathrm{d}}{\mathrm{d}z} g = \frac{\mathrm{sgn}(z)}{-2}\mathrm{e}^{\mathrm{i}k|z|}$, $\frac{\mathrm{d}^2}{\mathrm{d}z^2} g = -\delta(z) + \frac{\mathrm{i}k}{-2}\mathrm{e}^{\mathrm{i}k|z|}$.)

A.3 Green's Function for 3D Helmholtz Equation

Now consider $\Delta g + k_0^2 g = -\delta(\boldsymbol{x})$. To solve this, by taking Fourier transform w.r.t x and y to the equation, it leads to

$$(\Delta + k_0^2) \iint \mathrm{e}^{\mathrm{i}k_x x + \mathrm{i}k_y y} \hat{g}(k_x, k_y, z) \, \mathrm{d}k_x \, \mathrm{d}k_y = -\delta(z) \iint \frac{\mathrm{e}^{\mathrm{i}k_x x + \mathrm{i}k_y y}}{4\pi^2} \, \mathrm{d}k_x \, \mathrm{d}k_y$$

or equivalently

$$\frac{\partial^2}{\partial z^2} \hat{g} + k_z^2 \hat{g} = -\frac{\delta(z)}{4\pi^2} \qquad k_z^2 = k_0^2 - k_x^2 - k_y^2$$

By Green's function in 1D, we know $\hat{g}(k_x, k_y, z) = \frac{\mathrm{e}^{\mathrm{i}k_z|z|}}{-2\mathrm{i}k_z}$, and thus

$$g(\boldsymbol{x}) = \iint \frac{\mathrm{e}^{\mathrm{i}k_x x + \mathrm{i}k_y y + \mathrm{i}k_z|z|}}{-8\pi^2 \mathrm{i}k_z} \, \mathrm{d}k_x \, \mathrm{d}k_y = \frac{\mathrm{e}^{\mathrm{i}k_0\|\boldsymbol{x}\|}}{4\pi \, \|\boldsymbol{x}\|} \qquad \begin{array}{l} k_z = \sqrt{k_0^2 - k_x^2 - k_y^2} \\ \|\boldsymbol{x}\| = \sqrt{x^2 + y^2 + z^2} \end{array}$$

A.4 The Vector Green's Function

The Green's matrix $G(\boldsymbol{x}, \boldsymbol{x}') = \left[\left(I + \frac{\nabla\nabla}{k_0^2}\right) g(\boldsymbol{x}, \boldsymbol{x}')\right]$ for (30) has the Fourier integral representation

$$G(\boldsymbol{x}, \boldsymbol{x}') = -\iint_{\mathbb{R}^2} \frac{\mathrm{e}^{\mathrm{i}(k_x(x-x')+k_y(y-y')+k_z|z-z'|)}}{8\pi^2 \mathrm{i} k_z} \,\mathrm{d}k_x \,\mathrm{d}k_y$$

where $k_z = \sqrt{k_0^2 - k_x^2 - k_y^2}$ and

$$K = \begin{bmatrix} 1 - \frac{k_x^2}{k_0^2} & -\frac{k_x k_y}{k_0^2} & -\frac{k_x k_z}{k_0^2}\,\mathrm{sgn}(z-z') \\ -\frac{k_x k_y}{k_0^2} & 1 - \frac{k_y^2}{k_0^2} & -\frac{k_y k_z}{k_0^2}\,\mathrm{sgn}(z-z') \\ -\frac{k_x k_z}{k_0^2}\,\mathrm{sgn}(z-z') & -\frac{k_y k_z}{k_0^2}\,\mathrm{sgn}(z-z') & 1 - \frac{k_z^2}{k_0^2} + \frac{2\mathrm{i}k_z}{k^2}\delta(z-z') \end{bmatrix}$$

References

[1] F. Natterer, "An error bound for the Born approximation." *Inverse Problems* **20** (2004), 447-452.

[2] N. P. K. Cotter, T. W. Preist, and J. R. Sambles, "Scattering-matrix approach to multilayer diffraction." *J. Opt. Soc. Am. A* **12** (2004), 1097-1103.